ARTICLE IN PRESS

Available online at www.sciencedirect.com

ScienceDirect

ELSEVIER

Metabolic Engineering ▮ (▮▮▮▮) ▮▮▮–▮▮▮

METABOLIC ENGINEERING

www.elsevier.com/locate/ymben

Global metabolic changes following loss of a feedback loop reveal dynamic steady states of the yeast metabolome

Peng Lu[a,c,1], Anupama Rangan[c], Sherwin Y. Chan[b,2], Dean R. Appling[b,c], David W. Hoffman[b,c], Edward M. Marcotte[a,b,c,*]

[a]*Center for Systems and Synthetic Biology, University of Texas, 1 University Station, A4800, Austin, TX 78712-0159, USA*
[b]*Department of Chemistry and Biochemistry, University of Texas, 1 University Station, A5300, Austin, TX 78712-0159, USA*
[c]*Institute for Cellular and Molecular Biology, University of Texas, 1 University Station, A4800, Austin, TX 78712-0159, USA*

Received 3 October 2005; received in revised form 27 May 2006; accepted 20 June 2006

Abstract

Metabolic enzymes control cellular metabolite concentrations dynamically in response to changing environmental and intracellular conditions. Such real-time feedback regulation suggests the global metabolome may sample distinct dynamic steady states, forming "basins of stability" in the energy landscape of possible metabolite concentrations and enzymatic activities. Using metabolite, protein and transcriptional profiling, we characterize three dynamic steady states of the yeast metabolome that form by perturbing synthesis of the universal methyl donor *S*-adenosylmethionine (AdoMet). Conversion between these states is driven by replacement of serine with glycine + formate in the media, loss of feedback inhibition control by the metabolic enzyme Met13, or both. The latter causes hyperaccumulation of methionine and AdoMet, and dramatic global compensatory changes in the metabolome, including differences in amino acid and sugar metabolism, and possibly in the global nitrogen balance, ultimately leading to a G1/S phase cell cycle delay. Global metabolic changes are not necessarily accompanied by global transcriptional changes, and metabolite-controlled post-transcriptional regulation of metabolic enzymes is clearly evident.

Keywords: Metabolomics; Metabolic profiling; Nuclear magnetic resonance; Mass spectrometry; One carbon metabolism

1. Introduction

Living organisms are characterized by the quality of homeostasis, the tendency to maintain a constant internal state in response to varying external conditions. This tendency manifests itself particularly strongly in cellular metabolism. Such metabolic self-regulation leads not to equilibrium (cells are not closed systems), but to the adoption of dynamic steady states that represent the simultaneous satisfaction of all of the constraints present in the metabolic system (Fell, 1996). When components of such a system are perturbed, the system will re-equilibrate to a distinct dynamic steady state, adjusting all other components and rates to best accommodate the perturbation. On a rapid time scale, cells dynamically respond to the changing availability of metabolites by optimizing metabolite concentrations and enzyme activities in order to minimize the overall energy of the system, seeking out "basins of attraction" in a complex energy landscape.

In this paper, we describe the detailed experimental characterization of three such basins of stability in cellular metabolism, which occur as reproducible dynamic steady states of the cellular metabolic machinery, observed in response to perturbations to the synthesis of the universal methyl donor, *S*-adenosylmethionine (AdoMet). AdoMet is involved in methylating diverse substrates ranging from DNA and RNA to small molecules and amino acids, such

*Corresponding author. Department of Chemistry and Biochemistry, University of Texas, 1 University Station, A4800, Austin, TX 78712-0159, USA.
E-mail address: marcotte@icmb.utexas.edu (E.M. Marcotte).
[1]Current address: Departments of Genetics and Genomics, Roche, Palo Alto S3-1, 3431 Hillview Ave., Palo Alto, CA 94304, USA.
[2]Current address: Whitehead Institute for Biomedical Research, Massachusetts Institute of Technology, Nine Cambridge Center, Cambridge MA 02142-1479, USA.

1096-7176/$ - see front matter © 2006 Elsevier Inc. All rights reserved.
doi:10.1016/j.ymben.2006.06.003

as the lysine and arginine residues of histones, and is produced by activating methionine with ATP (Fontecave et al., 2004). We have investigated a system in which yeast cells can be forced to overproduce AdoMet by manipulating flux through the *MET13*-encoded methylenetetrahydrofolate reductase (MTHFR) enzyme. MTHFR catalyzes the reduction of 5,10-methylenetetrahydrofolate to 5-methyltetrahydrofolate, used to methylate homocysteine during methionine biosynthesis (Fig. 1). This is the committed step in methyl group biogenesis, with 5-methyltetrahydrofolate providing all the methyl groups of AdoMet in these cells.

We took advantage of a previously identified chimeric MTHFR (Chimera-1) composed of the yeast Met13p amino-terminal catalytic domain and the *Arabidopsis thaliana* MTHFR (AtMTHFR-1) carboxy-terminal regulatory domain (Roje et al., 2002). The resulting chimera is fully enzymatically active, but lacks the AdoMet-mediated feedback inhibition of the wild-type yeast enzyme and gains the ability to use reduced nicotinamide-adenine dinucleotide (NADH) as co-factor. Placement of Chimera-1 in a serine auxotroph (DAY4) produced an engineered strain (SCY4) with interesting properties: Cells grown in minimal media, but provided with serine, appear normal. However, replacement of serine with glycine and formate requires the cells to direct metabolic flux through the folate-mediated one-carbon pathways in order to meet their serine requirements (Fig. 1), leading to accumulation of greater than 100-fold more AdoMet and 7-fold more methionine than the wild type strain (Roje et al., 2002). These changes are accompanied by general reduction in growth rate of the cell (Chan and Appling, 2003), raising the question of what general molecular changes occur when

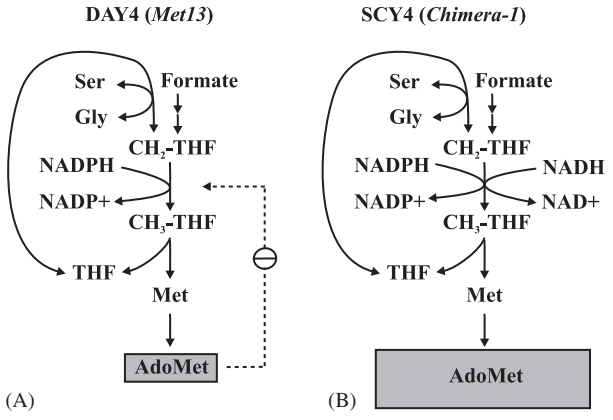

Fig. 1. Methyl group biogenesis in wild-type and engineered yeast strains. (A) In the wild-type strain DAY4 expressing Met13p, the MTHFR reaction is irreversibly driven towards CH_3-THF formation by a high cytosolic NADPH/NADP ratio. AdoMet overaccumulation is prevented by allosteric feedback inhibition of the MTHFR reaction (*dotted line*). (B) In strain SCY4 expressing the Chimera-1 MTHFR, AdoMet accumulates due to the lack of feedback inhibition by AdoMet. In addition, the capacity of the chimeric MTHFR to use NADPH as well as NADH results in more CH_3–THF synthesis and hence even greater AdoMet accumulation.

the nutritional status of these yeast is varied. By a combination of metabolic, transcriptional, and proteomic profiling, we characterize the phenotypes associated with these cells and demonstrate a reproducible global change in metabolic state upon removal of this single metabolic feedback loop, only poorly reflected in the accompanying transcriptional response. In total, we define three discrete dynamic steady states adopted by the yeast metabolome in response to variations in nutrition and one-carbon metabolism.

2. Materials and methods

2.1. Yeast strains and growth conditions

The *Saccharomyces cerevisiae* strains used were DBY8724 (*MAT*a *GAL2 ura3 bar1::URA3*) (Spellman et al., 1998), DAY4 (*MAT*a *ser1 ura3-52 trp1 leu2 his4*)(Roje et al., 2002) and SCY4 (*MAT*a *ser1 ura3-52 trp1 leu2 his4 Δmet13::CHIMERA-1*) (Roje et al., 2002). Yeast were grown in synthetic minimal medium (YMD medium) containing 0.7% yeast nitrogen base without amino acids (DIFCO Bacto), 2% glucose, supplemented with the following where indicated: L-serine (375 mg/L), L-leucine (30 mg/L), L-histidine (20 mg/L), L-tryptophan (20 mg/L), uracil (20 mg/L), glycine (20 mg/L), and formate (250 mg/L).

2.2. Metabolite extraction

Typically, 500 ml yeast cultures were harvested at mid-log phase, washed with PBS and re-suspended in 4% perchloric acid (50% wt/vol) (Shryock et al., 1986) with 9 μmol DSS (2,2-dimethyl-2-silapentane-5-sulfonic acid) as an internal reference. Samples were lysed by freezing and thawing twice, neutralized with KOH, and then centrifuged. The supernatants were dried by speed-vacuum and re-suspended in D_2O (Cambridge Isotope Laboratories, Inc.) for analysis. For the in vivo metabolite analysis, 1.5 L DBY8724 yeast cells were grown to mid-log phase. About 500 ml cells were used for soluble metabolome extraction; the remaining 1 L yeast were pelleted, washed, re-suspended, loaded directly into the NMR tube without lysis and analyzed intact. Comparison of 2D-NMR spectra from extracted metabolites with 2D-NMR spectra collected from intact yeast cells suggests that only minimal bias in the metabolite population is introduced by the sample preparation (data not shown).

2.3. NMR data acquisition, processing and resonance assignments

NMR spectra were recorded at 30 °C using a 500 MHz Varian Inova spectrometer equipped with a triple resonance probe and *z*-axis pulsed-field gradient. Resonances were assigned using proton detected correlated spectroscopy (COSY and TOCSY), carbon 1D spectra,

and ^{1}H-^{13}C single-bond correlated HSQC spectra. Peaks used in the quantitative metabolite analyses were picked from 2D ^{1}H-^{13}C HSQC spectra acquired using *z*-axis pulsed field gradients for coherence selection, ^{1}H and ^{13}C sweep widths of 6000 and 25000 Hz, respectively, and ^{13}C decoupling during the acquisition time. Spectra were acquired using 16–64 scans per FID, 2048 and 512 points for the ^{1}H and ^{13}C dimensions, and total spectrum acquisition times of 2.75–11 h. Tentative NMR assignments were confirmed by acquiring spectra of samples spiked with purified compounds. 2D-NMR spectra were processed with NMRPipe (Delaglio et al., 1995) and interpreted with the aid of the Sparky Assignment and Integration Software package (http://www.cgl.ucsf.edu/home/sparky). After all peaks were picked, assigned and integrated, peak heights were normalized by the peak heights of the DSS internal reference standard and the wet sample weights. Linearity of response was tested by adding analytes of known concentration to wild-type yeast extracts and collecting corresponding data. Following each addition, peak heights were normalized using an internal DSS control to correct for minor sample volume variations. Clustering and principle component analysis of metabolite profiles were performed with the programs Cluster and Treeview (Eisen et al., 1998).

2.4. mRNA and protein preparation

Proteins and mRNA were harvested from the yeast strains DAY4 and SCY4, isolating mRNA and proteins from biological replicate yeast cultures grown under the same conditions. Starter cultures were grown in YMD medium containing serine, diluted to O.D. 0.05 in either the same serine-containing medium or YMD medium containing glycine and formate, then grown to mid-log phase at 30 °C. From one set of the cultures, total RNA was extracted using phenol/chloroform, poly(A) RNA was purified, and cDNA was synthesized by reverse-transcription as described previously (Spellman et al., 1998). Protein was harvested from the other set of cultures via bead-beating as described previously (Xue et al., 2000).

2.5. DNA microarray analysis

The synthesized cDNA was hybridized to a DNA microarray containing all of the intergenic and predicted coding regions of the yeast genome manufactured as described previously (Hahn et al., 2004; Kim and Iyer, 2004). The resulting microarrays were scanned with a GenePix 4000B scanner (Axon Instruments) and quantified with GenePix 5.0 software. Data were uploaded into the LAD microarray database (Killion et al., 2003) and filtered to pass minimum quality control thresholds (sum of median intensities >300 and regression correlation across spot pixels >0.6) before further analysis.

2.6. LC/LC/MS/MS analysis

Soluble protein extracts were diluted in digestion buffer (50 mM Tris HCL pH 8.0, 1.0 M Urea, 2.0 mM $CaCl_2$) to 4 mg/ml, denatured at 95 °C for 10 min, and digested with sequencing grade trypsin (Sigma) at 37 °C for 20 h. Tryptic peptide mixtures were separated by automated two-dimensional high-performance liquid chromatography. Chromatography was performed at 2 μl/min with all buffers acidified with 0.1% formic acid. Chromatography salt step fractions were eluted from a strong cation exchange column (SCX) with a continuous 5% acetonitrile (ACN) background and 10 min salt bumps of 0, 20, 60 and 900 mM ammonium chloride. Each salt bump was eluted directly onto a reverse phase C18 column and washed free of salt. Reverse phase chromatography was run in a 125 min gradient from 5% to 55% ACN, and then purged at 95% ACN.

Peptides were analyzed online with electrospray ionization (ESI) ion trap mass spectrometry (MS) (Link et al., 1999; Washburn et al., 2001) using a ThermoFinnigan Surveyor/DecaXP+ instrument. In each MS spectrum, the six tallest individual peaks, corresponding to peptides, were fragmented by collision-induced dissociation (CID) with helium gas to produce MS/MS spectra. Gas phase fractionation (GPF) was used to achieve maximum proteome coverage (Yi et al., 2002). In order to increase coverage of lower abundance proteins, each tryptic peptide mixture was analyzed by three sequential LC/LC/MS/MS analyses, in each case examining a different mass/charge (m/z) range (300–650, 650–900, and 900–1500 m/z) for data-dependent precursor ion selection for CID; fragmentation data from the three runs were then combined for analysis. Proteins were identified from the resulting peptide MS/MS fragmentation spectra using Bioworks TurboSequest (Eng et al., 1994), PeptideProphet (Keller et al., 2002), and ProteinProphet (Nesvizhskii et al., 2003). The probability of correctly identifying each protein and its individual spectral counts in a given proteomics experiment was calculated using ProteinProphet.

For the purpose of generating clusters in Fig. 6, a ProteinProphet probability threshold of 0.2 was chosen for protein identification, and spectral counts were treated as a rough, order-of-magnitude measure of protein expression levels (Liu et al., 2004). Differential protein expression was calculated using the APEX scheme (Lu et al., manuscript submitted) as a Z-score based on numbers of spectral counts ($n_{i,1}$ and $n_{i,2}$) observed for a given protein i between two experiments with N_1 and N_2 total spectral counts each, calculated as

$$Z = \frac{f_{i,1} - f_{i,2}}{\sqrt{f_{i,0}(1-f_{i,0})/N_1 + f_{i,0}(1-f_{i,0})/N_2}},$$

where $f_{i,1}$ and $f_{i,2}$ are the fractions of spectral counts for protein i in experiments 1 and 2 (equal to $n_{i,1}/N_1$ and $n_{i,2}/N_2$, respectively), and the denominator represents

the standard error of the difference under the null hypothesis in which the two sampled proportions are drawn from the same underlying distribution with the overall proportion $f_{i,0} = (n_{i,1} + n_{i,2})/(N_1 + N_2)$. Proteins with $|Z| > 2.58$ and > 1.96 were considered significantly differentially expressed at the 99% and 95% confidence levels, respectively.

2.7. FACS analysis

The yeast cells were grown in YMD media containing serine or glycine and formate. Cell cultures were harvested at mid-log phase, then assayed for DNA content by staining with the DNA-specific dye propidium iodide, followed by flow cytometry with a BD Biosciences FACSCalibur instrument using standard protocols.

3. Results and discussion

3.1. Quantifying metabolites by ^{1}H-^{13}C 2D-NMR

In order to metabolically profile the yeast cells as their growth conditions and nutritional status were varied, we applied ^{1}H-^{13}C two-dimensional nuclear magnetic resonance (2D-NMR). In comparison with ^{1}H-NMR (Raamsdonk et al., 2001; Viant et al., 2003), ^{1}H-^{13}C multinuclear NMR (Szyperski et al., 1999; Lindon et al., 2003) greatly reduces the overlap between peaks in each spectrum (Viant, 2003), allowing their accurate identification and quantitation. Fig. 2 shows sections of the ^{1}H-^{13}C 2D-NMR spectrum of a DAY4 yeast cell extract. 200 NMR peaks were consistently observed across all spectra. In order to positively identify the corresponding compounds, we

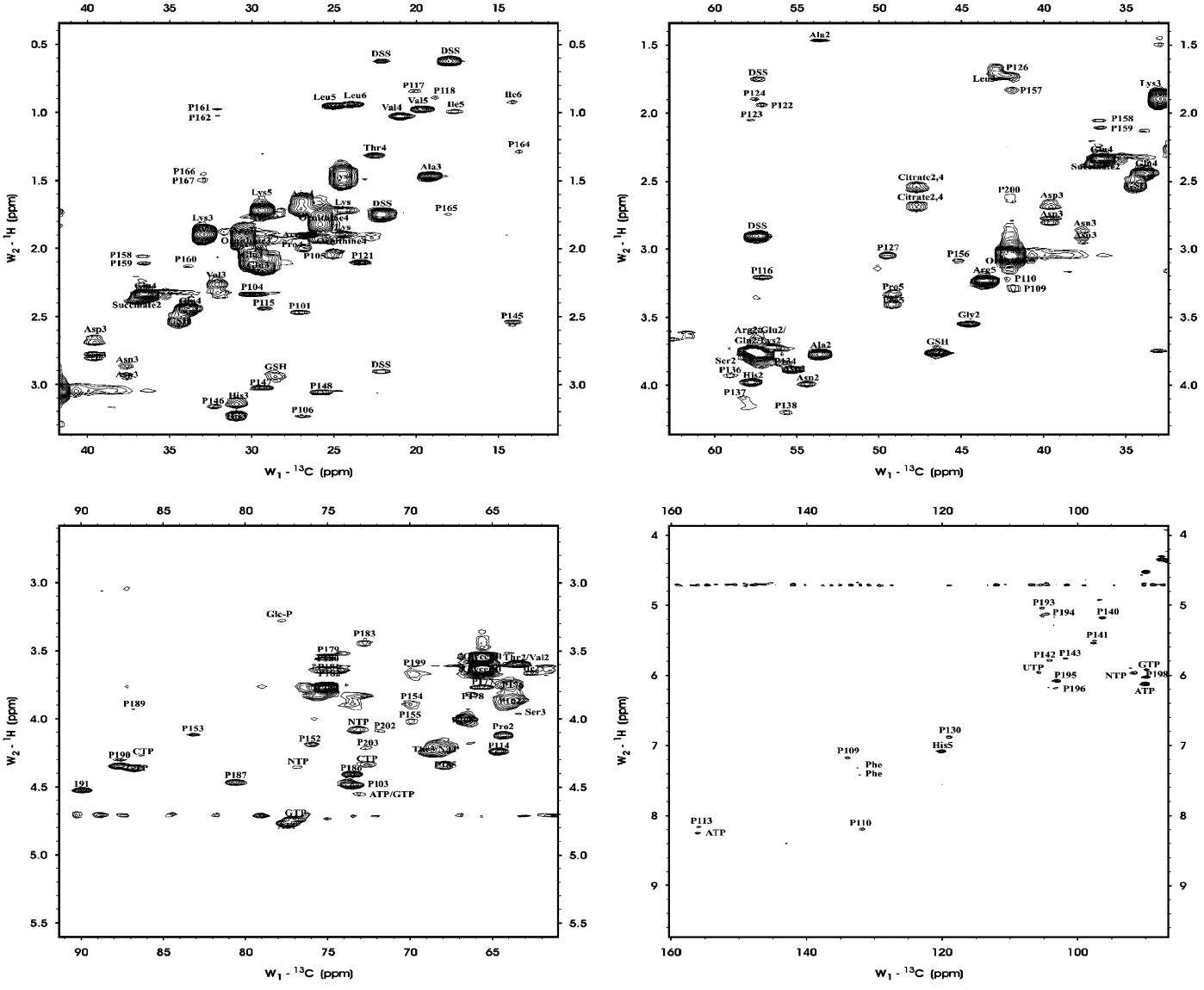

Fig. 2. Metabolic profiling by 2D-NMR. Sections are plotted of an ^{1}H-^{13}C correlated HSQC NMR spectrum of the DAY4 yeast metabolome. Assignments of labeled compounds were verified by spiking experiments. Peaks labeled by P# are measured but unassigned to specific compounds. A complete list of resonance assignments and chemical shifts is provided as Supplemental Table 1.

assigned the resonances using COSY, TOCSY and carbon 1D experiments in addition to ^{1}H-^{13}C 2D-NMR. Altogether, identities of 94 peaks were assigned and corresponded to 30 distinct metabolites, including amino acids, monosaccharides, nucleotides and various other small molecules. The remaining 106 peaks were consistently observed and measured but unassigned, indicating that a total of ~60–136 total metabolites were monitored by this approach. The higher value is more probable as no cross-correlations were observed among the unassigned peaks in COSY and TOCSY experiments, implying these peaks derive from distinct metabolites. The complete set of resonance assignments, each verified by spiking experiments, is listed as Supplementary Table 1.

To be useful for metabolite profiling, ^{1}H-^{13}C 2D-NMR must be both quantitative and reproducible. To test the correlation between ^{1}H-^{13}C 2D-NMR signal intensities and metabolite abundance, we spiked yeast cell extracts with known amounts of reference compounds and measured the changes in metabolite peak heights. As shown in Fig. 3A, the NMR peak heights vary linearly with the abundance of metabolites in the sample and this linear relationship exists over at least three orders of magnitude of concentration. Tests with amino acids, carbohydrates, nucleotides and other metabolites gave similar results (data not shown). From spiking experiments such as these, the absolute amount of a metabolite in the sample can be obtained (Fig. 3A), and by correcting for cell mass, the absolute cellular concentration of the metabolite can be estimated. For example, we observed ~76 μg histidine in wild-type yeast samples—based on the cell mass analyzed (~0.6 g), this implies the cellular histidine concentration is roughly 0.5 mM, assuming the accessible volume of a typical yeast cell is 0.6 ml/g (Arnold and Lacy, 1977). Previously measured concentrations of cellular histidine are comparable (1.6 mM (Strathern et al., 1982)) within the variance expected between different yeast strains. The estimated sensitivity of ^{1}H-^{13}C 2D-NMR based on detection of the internal control is ~50 μM, using a conventional 500 MHz spectrometer, the natural abundance of ^{13}C, and a data collection time of 11 h. To examine reproducibility, we compared quantitation of NMR peak heights from 12 pairs of biological replicate metabolome samples (2400 peak pairs in total), which is shown in Fig. 3B. Quantitation was highly reproducible ($R^2 = 0.95$), demonstrating that the variability introduced by sample preparation and ^{1}H-^{13}C 2D-NMR measurement is minimal and compares favorably to metabolic profiling by gas chromatography/mass spectrometry (Fiehn et al., 2000).

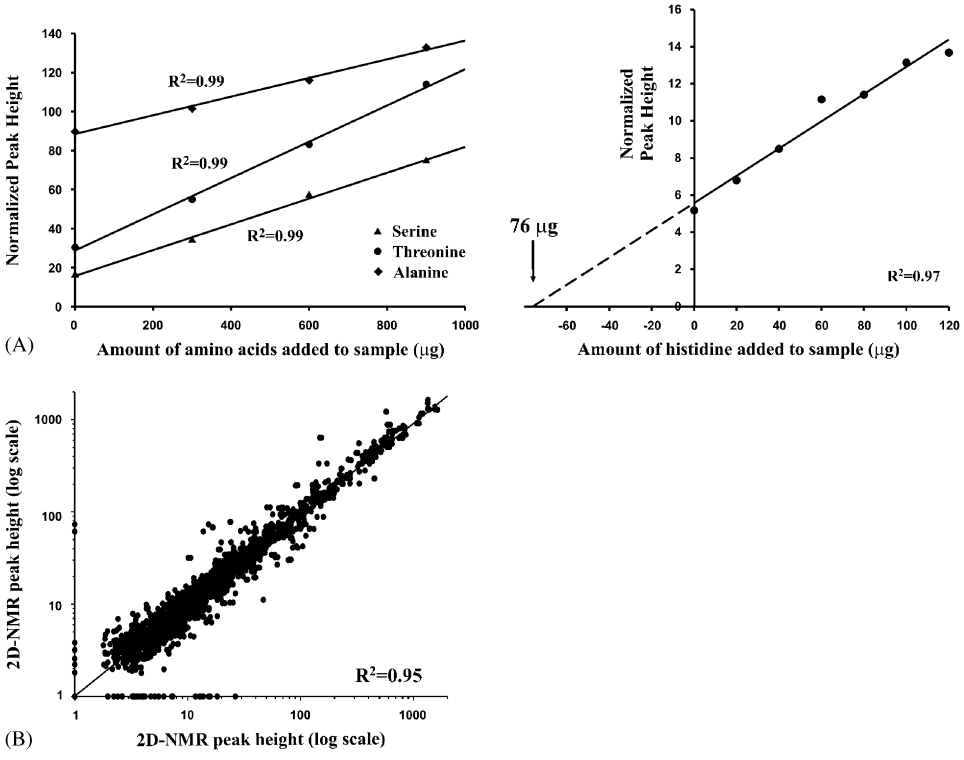

Fig. 3. Linearity and reproducibility of the 2D-NMR metabolite measurements. Peak heights in 2D NMR spectra vary linearly with metabolite concentration over at least three orders of magnitude and are highly reproducible: (A) Spiking of a yeast lysate with known amounts of three amino acids shows that the 2D-NMR peak heights increase linearly with the amount of compound added. In the right plot, the x-intercept of the peak height-concentration curve reveals the absolute amount of histidine present in the original sample. Correcting for the estimated cell mass in the sample tube gives an absolute cellular concentration of ~500 μM histidine. (B) Comparison of the measured peak heights for 200 2D-NMR peaks from 12 pairs of biological replicate metabolome samples (2400 comparisons in total) demonstrates the high reproducibility of 2D-NMR metabolic profiling. Note that, occasionally, a peak is not observed in a replicate experiment (falling here on the x and y axes), placing the false negative observation rate of the technique at ~42 of 2400 observations, or 2%, for this set of NMR peaks.

3.2. Detailed metabolome analysis of a yeast metabolic mutant

In order to gain insight into the metabolic states of the one carbon metabolism mutants, wild type *MET13* yeast (DAY4) and the Chimera-1 mutant SCY4 were grown separately to mid-log phase in serine or glycine + formate media and their lysates were analyzed by ^{1}H-^{13}C 2D-NMR. The data were then normalized and organized via hierarchical clustering, an approach common for microarray-based mRNA expression surveys (Eisen et al., 1998). The metabolic profiles are plotted in Fig. 4, with both rows and columns ordered according to the hierarchical clustering of metabolic profiles and sample profiles, respectively. Several broad patterns are evident in the metabolomes. First, replicate samples tend to have similar metabolomes (columns in Fig. 4), indicated by their tendency to cluster together by their metabolic profiles. Second, the primary division between the samples correlates with their growth media, indicating that nutritional status plays the dominant role in determining the metabolomes. Third, in serine medium, there are only subtle differences between the metabolite profiles of DAY4 and SCY4, while the differences become much more prominent in the glycine + formate medium. This correlates with the previous observation that the growth rates of these two strains were similar in serine minimal medium, yet the doubling time of SCY4 was nearly twice as long as DAY4 in

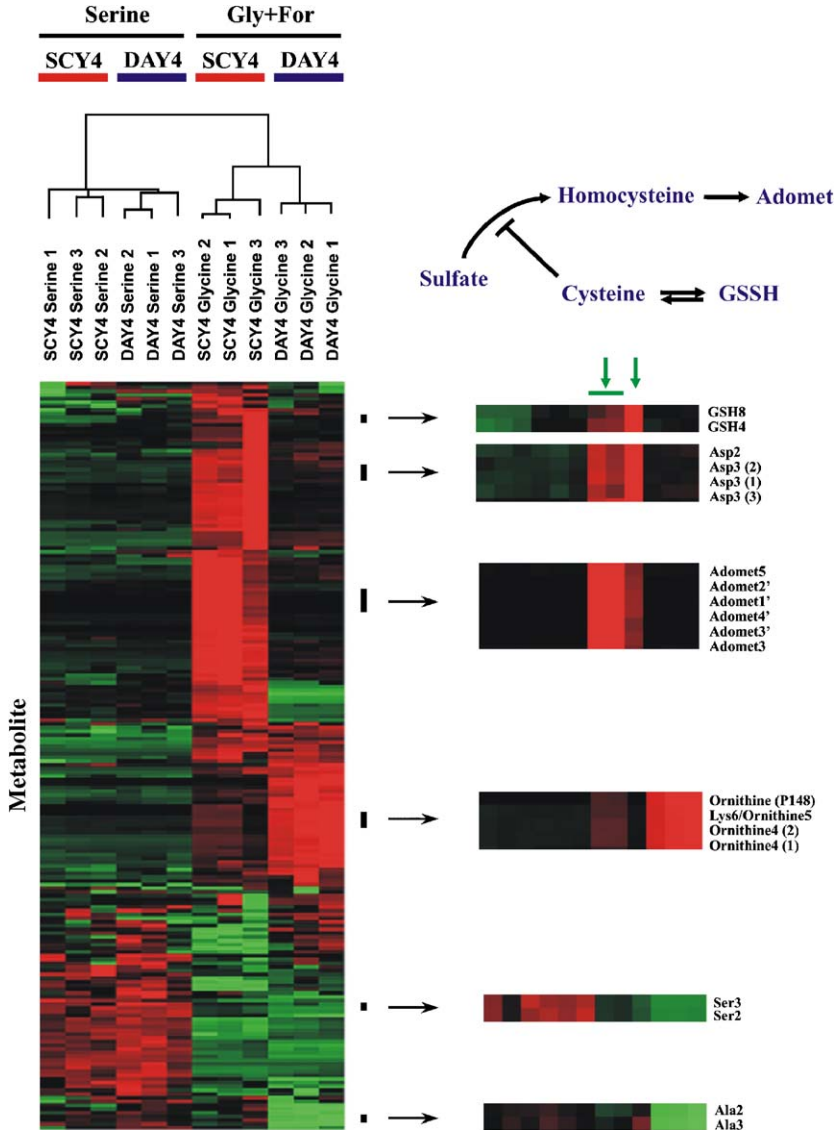

Fig. 4. Variation between the cells' internal metabolic states is demonstrated by unsupervised hierarchical clustering of DAY4 and SCY4 metabolic profiles in different nutritional states. Each row corresponds to a single 2D-NMR metabolite peak, with columns representing strains/experimental conditions (each strain/condition analyzed in triplicate). The normalized magnitude of each 2D-NMR peak height is indicated by color, with red indicating an increase in metabolite abundance compared with the median abundance of that metabolite across all samples, green indicating a corresponding decrease in abundance, and black for the median level of abundance. Variations within SCY4 glycine + formate replicates (green arrows) apparently derive from feedback inhibition of cysteine on homocysteine synthesis (Chan and Appling, 2003), diagrammed on the top right. Absent data or data of low quality were filled by the NMR peak background threshold level.

glycine + formate medium (Chan and Appling, 2003). Fourth, hierarchical clustering of the metabolites by their abundance profiles across samples (rows in Fig. 4) indicates that NMR peaks derived from the same metabolites cluster together, demonstrating the accuracy and reproducibility of ^{1}H-^{13}C 2D-NMR for metabolomic profiling. As metabolites responding in a similar fashion across samples also cluster together, the hierarchical clustering captures major trends in metabolic flux between the samples, as discussed later in more detail.

As expected, engineered yeast (SCY4) expressing the chimeric MTHFR are insensitive to AdoMet inhibition in vivo and accumulate much more AdoMet and methionine than the wild type (Roje et al., 2002). However, this phenomenon was not observed when the supplemental glycine and formate were replaced by serine in the culture medium (Chan and Appling, 2003). Correspondingly, the AdoMet peak is large in the SCY4-Gly + For spectra, but undetectable in DAY4-Gly + For, DAY4-Ser and SCY4-Ser spectra. Likewise, the methionine peak height in SCY4-Gly + For spectra is about 5.5-fold higher than that in DAY4-Gly + For spectra; there is no significant difference in methionine abundance between these two strains in the serine medium.

The relative abundance changes in known metabolites across the experiments are summarized in Fig. 5, and a number of more detailed trends in the cells' metabolomes can be seen, in particular in amino acid metabolic pathways. For example, lysine was elevated in the glycine + formate-enriched medium, especially in DAY4 cells. Lysine and homocysteine represent the two major downstream branches of the aspartate biosynthesis pathway. Aspartate was abundant in both DAY4-Gly + For and SCY4-Gly + For samples, suggesting that the aspartate pathway is up-regulated when glycine is provided as a C_1 carbon source. In SCY4, the AdoMet-insensitive chimeric MTHFR ensures high levels of CH_3-THF for the methylation of homocysteine to methionine and AdoMet (Roje et al., 2002). In wild type cells, AdoMet feedback inhibits MTHFR activity so that CH_3-THF levels are low, and thus homocysteine methylation is slowed. As flux from pyruvate to aspartate increases, alanine, valine and isoleucine synthesis from pyruvate are decreased. Acetate is also higher in the glycine + formate-grown cells. Although acetate can be produced from pyruvate, it is also generated from threonine. Threonine, which derives from aspartate via homoserine, was also elevated in SCY4-Gly + For cells. Threonine is then cleaved by threonine

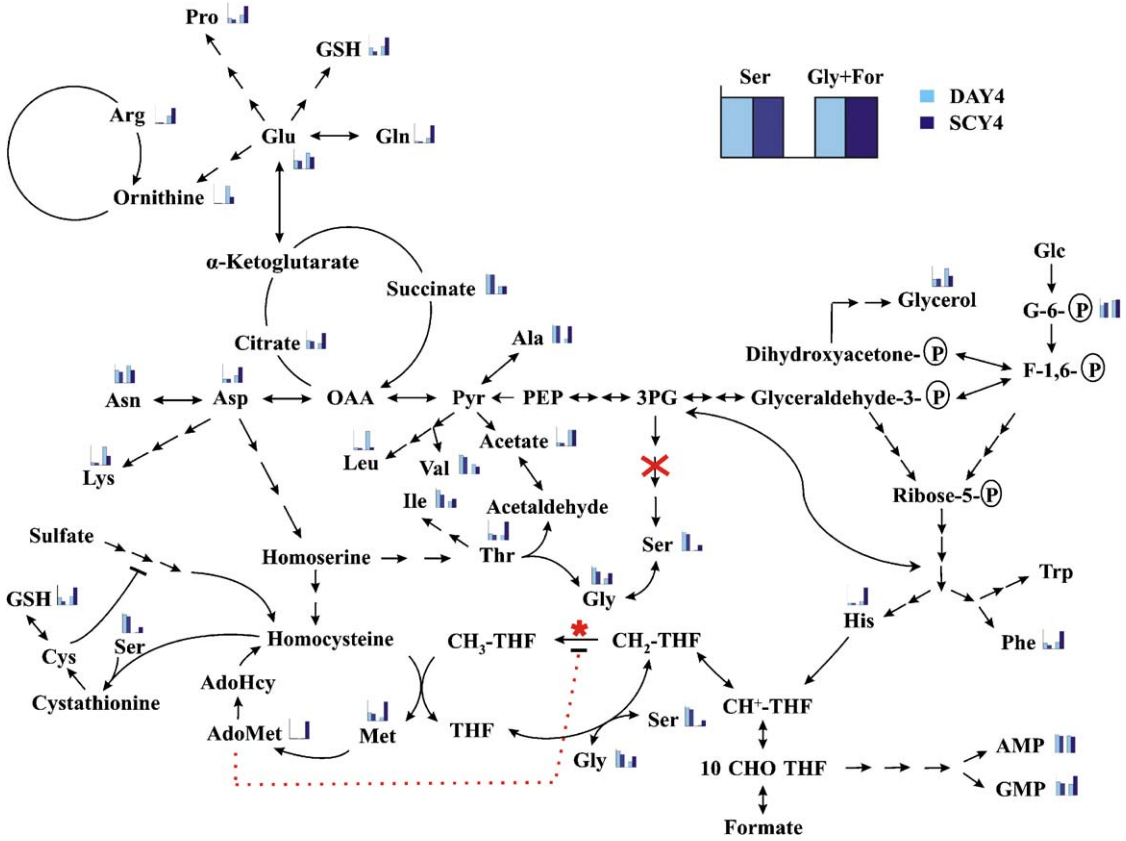

Fig. 5. Summary of global metabolome changes to yeast one-carbon metabolism and related pathways. Red X indicates the inactivated phosphoserine aminotransferase in both DAY4 and SCY4 strains; red * indicates chimeric MTHFR (Methylenetetrahydrofolate reductase) in SCY4 strain; solid black line indicates the regulation existing in both DAY4 and SCY4 strains; dashed red line indicates the regulation only existing in DAY4 strain. All bars show the normalized abundances of measured metabolites, averaged across three biological replicates for SCY4 and DAY4 cells growing in either Ser or Gly + For media.

aldolase to produce glycine and acetaldehyde, which is in equilibrium with acetate (McNeil et al., 1994; Woldman and Appling, 2002). Thus, it appears that in glycine + formate medium, flux from aspartate towards lysine and homoserine increases, leading to increased threonine and homocysteine (and subsequently AdoMet) synthesis.

A second major trend is revealed by considering the levels of histidine. Histidine also contributes C_1 units through its degradation with formation of N^5-forminino-THF. Since SCY4 has an unregulated MTHFR and there is no serine inhibition in glycine + formate medium, all of the formate is taken up through the *ADE3* gene product to make 5,10-CH_2-THF and ultimately, 5-CH_3-THF. As 5,10-methenyl-THF is an intermediate between formate and 5,10-CH_2-THF, it is possible that SCY4, which may have greater flux through Ade3p, might decrease the use of histidine in order to make 5,10-methenyl-THF in the glycine + formate medium.

As reported by Chan and Appling (2003), serine represses AdoMet hyperaccumulation in SCY4 by a variety of mechanisms. Serine can deplete the homocysteine pool by condensing with homocysteine to form cystathionine, thereby limiting the amount of methionine and AdoMet synthesized. In addition, serine acts to repress the biosynthesis of homocysteine through its role in the synthesis of cysteine (Vanaerts et al., 1994; Chan and Appling, 2003). When serine is absent in the medium, it can only be synthesized via serine hydroxymethyltransferase (SHMT) because the conversion of 3-phosphoglycerate to serine is blocked at phosphoserine aminotransferase in these strains. Therefore, in glycine + formate medium, the low intracellular serine levels (Fig. 5) are apparently adequate to meet growth requirements, but not high enough to repress AdoMet synthesis.

We also observe potential changes in the global nitrogen balances of the cells, with arginine levels favored over ornithine in the SCY4-Gly + For cells and glutamine favored over glutamate. However, this ratio is inverted with aspartate and asparagine, arguing that a different mechanism may also account for the skewed ratios of glutamine/glutamate and arginine/ornithine.

3.3. Combination of transcriptome, proteome and metabolome

To test if changes in the metabolome were accompanied by changes in the transcription and translation of metabolic enzymes or regulated proteins [e.g., as in Ideker et al. (2001)], we profiled the cells' transcriptomes and proteomes with DNA microarrays (Lockhart and Winzeler, 2000) and mass spectrometry (Aebersold and Mann, 2003), respectively. We expected that a comparison of data across the three levels would allow us to better describe the cells' states, characterizing the entire biological system more comprehensively and giving insight into the extent to which perturbation- or nutrition-induced changes in gene expression and metabolite levels were correlated. We profiled ~800 proteins expressed by these cells with high confidence via the use of "MudPit" style (Washburn et al., 2001) multi-dimensional high-performance liquid chromatography and tandem mass spectrometry (LC/LC/MS/MS), and profiled the complete set of mRNA transcripts via the use of cDNA microarrays (Iyer, 2003; Hahn et al., 2004; Kim and Iyer, 2004). The complete sets of transcript and protein profiles are listed in Supplemental Tables 2 and 3, respectively. Fig. 6 shows the resulting transcriptional and proteomic profiles after hierarchical clustering. As for the metabolite profiles, the primary division among the samples at the transcriptome and proteome levels is by nutritional status. However, the transcriptomes of the SCY4 and DAY4 appear more similar than either their proteomes or metabolomes would imply, consistent with the critical role of post-transcriptional regulation for both

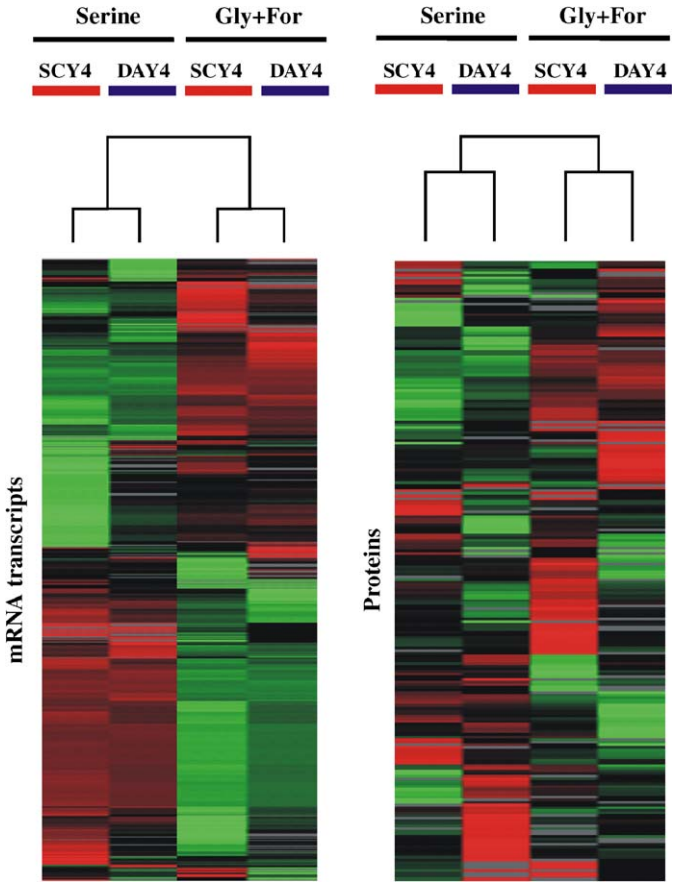

Fig. 6. Transcriptional and proteomic profiles of DAY4 and SCY4 in different nutritional states, shown by unsupervised hierarchical clustering. In the transcriptional profiles (left diagram), rows correspond to genes and columns to strains/experimental conditions. Colors indicate the magnitude of induction/repression for each gene relative to the pooled mRNA from all samples. In the proteomic profiles (right diagram), rows correspond to proteins columns to strains/experimental conditions. Colors indicate the spectral counts of each protein, an approximate measure of protein abundance (Liu et al., 2004), normalized by the protein's median abundance across all samples. In both plots, red indicates an increase in abundance compared with the median across the samples, green indicates a decrease in abundance, and black indicates the median abundance. Missing data are plotted in gray. In each plot, only genes/proteins observed in at least three of the four samples are plotted.

protein and metabolite levels (Parekh and Rohlff, 1997; Griffin et al., 2002).

Such post-transcriptional regulation is indeed evident in the profiling data. The MTHFR feedback inhibition is one example. Another such example, illustrated in Fig. 7, is that of the arginine biosynthesis enzyme, carbamoylphosphate synthase (CPSase A). CPSase A is composed of two subunits, CPA1 and CPA2, known to be subject to two different regulatory mechanisms (Messenguy et al., 1983). While transcription of both the *CPA1* and *CPA2* mRNAs are regulated by the transcription factor GCN4 in response to general amino acid starvation, the CPA1p protein is additionally repressed by arginine via upstream open reading frames (Werner et al., 1987; Delbecq et al., 1994). At the mRNA level, we see no obvious change in the mRNA abundance of either *CPA1* or *CPA2* in serine media relative to glycine + formate media (Fig. 7). At the protein level, the CPA2 protein is present in both conditions (measured as the probability of identification). By contrast, the CPA1 protein, while clearly detectable in serine media, is undetectable in glycine + formate media. (Here, we rely upon the tendency for confidence in protein identification to serve as a surrogate for protein abundance (Ishihama et al., 2005; Wang et al., 2005); more formally, it indicates a lack of positive evidence for the presence of *CPA1*.) Thus, it appears *CPA1* is down-regulated at a post-transcriptional level in the SCY4 glycine + formate cells. The loss of CPA1 protein agrees with the increase in concentration (roughly doubling) of arginine in the cells, consistent with the known mode of *CPA1* regulation (Werner et al., 1987; Delbecq et al., 1994).

Nonetheless, the primary transcriptional and translational changes do pertain specifically to metabolism. In either the SCY4 or DAY4 cells, when switched between Ser and Gly + For media, mRNAs differentially expressed more than 2-fold are entirely dominated by amino acid biosynthetic enzymes, statistically enriched ($P<10^{-9}$, calculated via FunSpec (Robinson et al., 2002)) for genes with the Gene Ontology annotations amino acid metabolism, amino acid and derivative metabolism, amine metabolism, amino acid biosynthesis, and amine biosynthesis, with both strains showing differential expression of, for example, *ARO3, ARO9, ARO10, TRP4, GLY1, SER3, STR3, ARG4, PUT2, ECM40, HIS3, HIS5,* and *CAR1*. Additionally, DAY4 cells show differential expression of genes of sulfur amino acid metabolism, methionine metabolism and sulfur metabolism (in particular, *MET32, HOM3, CYS4, MET14, MET1, MET17, MET2,* and *MET22*), and aspartate family amino acid metabolism. The only significant ($P<10^{-6}$) expression change between SCY4 and DAY4 cells grown in Gly + For are four genes of one-carbon compound metabolism (*GCV1, GCV2, FDH1,* and *FDH*2). No significantly different GO biological processes were detected among genes expressed more than 2-fold between DAY4 and SCY4 cells grown in Ser media, a trend also reflected by their similar metabolic profiles.

At the protein level, the predominant difference in the proteomes of SCY4 and DAY4 cells in Ser media are not due to metabolic proteins, but instead in the protein synthesis apparatus, with the most strongly differentially expressed proteins ($P<10^{-14}$ for proteins differentially expressed at the 99% confidence level) corresponding to the Gene Ontology biological process annotation protein biosynthesis. Likewise, at the protein level, the strongest differentially expressed pathway observed between SCY4 and DAY4 cells grown in Gly + For media is again not metabolic, but a difference in protein folding ($P<10^{-6}$), in particular the proteins SSA1, HSC82, and HSP82, presumably a reflection of the growth difficulties experienced by the SCY4 strain. However, within either strain, the shift from Ser to Gly + For brings predominantly changes in metabolic protein expression levels, with either strain showing elevated SER3, SER33, and ARG4 protein levels in Gly + For media, and elevated ILV5, LYS21, ALD6, and ADH1 protein levels in Ser media. These changes are detailed in full in Supplemental Table 3.

3.4. Hyperaccumulation of AdoMet delays the G1-to-S phase cell cycle transition

AdoMet is the most commonly used enzyme cofactor after ATP, the nicotinamide dinucleotides, and CoA (Forster et al., 2003), and the alteration of its cellular

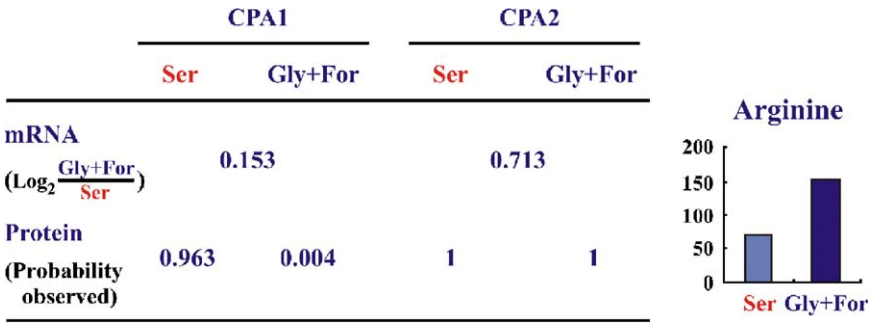

Fig. 7. Detection of metabolite-controlled post-transcriptional regulation in the *SCY4* strain. In glycine + formate media, the arginine concentration is approx. twice that in serine media (right graph). While the mRNA levels of arginine biosynthesis gene *CPA1* are essentially unchanged in the two conditions (shown at left), the protein is observed only in the serine media, i.e., when arginine is low, consistent with post-transcriptional regulation of *CPA1* protein levels (Messenguy et al., 1983). By contrast, the arginine biosynthesis gene *CPA2* shows no such arginine-mediated translational repression.

concentration has profound effects on cell growth although the detailed mechanism producing these effects is still unclear. In order to better characterize the defect associated with AdoMet overproduction, we attempted to explain the increased doubling time of the SCY4 glycine cells [roughly twice that of DAY4 glycine cells (Chan and Appling, 2003)] by searching for a cell cycle-related defect. As expression deconvolution analysis (Lu et al., 2003) can in principle reveal the precise nature of cell cycle defects in mutant cells, we analyzed the mRNA expression profiles of DAY4 and SCY4 cells to search for patterns typical of cell cycle defects. As illustrated in Fig. 8A, DAY4 cells showed transcriptional profiles characteristic of roughly equal proportions of cells in different cell cycle phases, but SCY4 cells in glycine + formate minimal medium exhibited a strong bias toward transcription characteristic of G_1 phase, suggesting a rate-limiting defect in their cell cycles.

To validate the expression deconvolution results, we assayed the distribution of the cells throughout the cell cycle via fluorescence-activated cell sorting (FACS), measuring the numbers of cells with one (1N) and two (2N) copies of the chromosomes. The FACS data confirm that SCY4 cells in glycine + formate minimal medium show excess 1N cells and are delayed in G_1 phase (Fig. 8B). This observation supports the notion that the accumulation of AdoMet in vivo can cause G_1 cell cycle delay, just as does addition of exogenous AdoMet (Mizunuma et al., 2004).

However, in contrast to adding exogenous AdoMet, whose effects appear to be mediated by down-regulating *SWE1* and *CLN2* expression (Mizunuma et al., 2004), hyperaccumulation of AdoMet in SCY4 cells does not affect the mRNA abundance of *SWE1* and *CLN2* ($\log_2(SWE1)_{\mathrm{Gly+For/Ser}} = -0.21$; $\log_2(CLN2)_{\mathrm{Gly+For/Ser}} = 0.14$). Other lines of evidence also suggest a different mechanism of cell cycle delay, with indirect evidence suggesting the possibility that overproduction of polyamines might be involved in the cell cycle delay observed in *SCY4* cells. Polyamines are known to be critical for cell cycle progression, with either too low or too high levels causing cell cycle delays in yeast (Kay et al., 1980; Balasundaram et al., 1991; Schwartz et al., 1995). In other eukaryotic cells, polyamines are known to induce G_1 cell cycle delay by post-translational modification of eIF-5A (Chan et al., 2002). AdoMet and ornithine are two major precursors in the polyamine biosynthesis pathway. Although polyamines were not directly observed in the experiment, ornithine was strongly depleted under conditions of AdoMet hyperaccumulation, suggesting that polyamine synthesis was active. In addition, the mRNA expression levels of *TPO2* and *TPO4*, two vacuolar polyamine transporters (Tomitori et al., 2001), are markedly induced in response to the elevated AdoMet levels, further suggesting altered polyamine metabolism in cells that hyperaccumulate AdoMet. Confirmation of this hypothesis will require direct measurements of polyamine levels by other analytical methods, but this represents another example of the power of the global approach described here.

3.5. Basins of metabolic stability

The broad trends in the data are more apparent after principle component analysis (PCA), which organizes the samples according to the major sources of variation in the data (Duda et al., 2001). Plotting the samples according to the PCA analysis (Fig. 9) again shows that biological replicates cluster most strongly, the DAY4 and SCY4 cells in serine media appear to have similar metabolomes, but shifting to glycine + formate media induces significant changes to each metabolome. The first principle component, capturing the largest source of variance in the data, corresponds to media-dependent metabolism changes. The second principle component captures Met13/Chimera-1 (genotype)-dependent changes.

	DAY4		SCY4	
	Ser	Gly+For	Ser	Gly+For
% G1	33.33	50	30.8	100
% S	0	50	0	0
% G2	33.33	0	38.5	0
% M	0	0	7.7	0
% M/G1	33.33	0	23.1	0

(A)

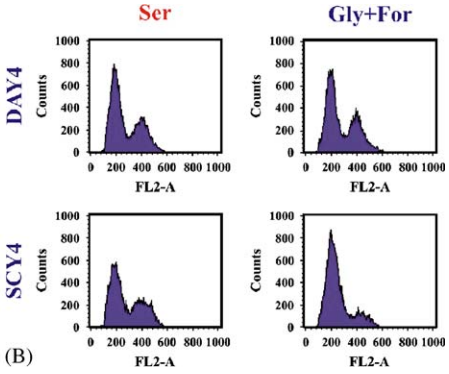

(B)

Fig. 8. Evidence for a G1/S phase cell cycle delay associated with accumulation of AdoMet. (A) Expression deconvolution of DAY4 and SCY4 cell transcriptional profiles indicates a G_1-phase delay for SCY-glycine/formate cells. The predicted proportion of cells in each phase of the cell cycle, measured by expression deconvolution analysis (Lu et al., 2003) of their transcriptional profiling data, show that DAY4 cells have roughly equal proportions of cells in different cell cycle phases, but SCY4 cells in glycine + formate minimal medium exhibit a strong bias toward G_1 phase, suggesting a rate-limiting defect in their cell cycles. (B) FACS analysis validates the cell cycle defect for SCY4 cells in glycine + formate minimal medium. Compared with the distribution of asynchronous DAY4 cells and SCY4 cell in serine minimal medium, FACS data confirm that asynchronous SCY4 cells in glycine + formate minimal medium show excess 1N cells and are delayed in G_1 phase.

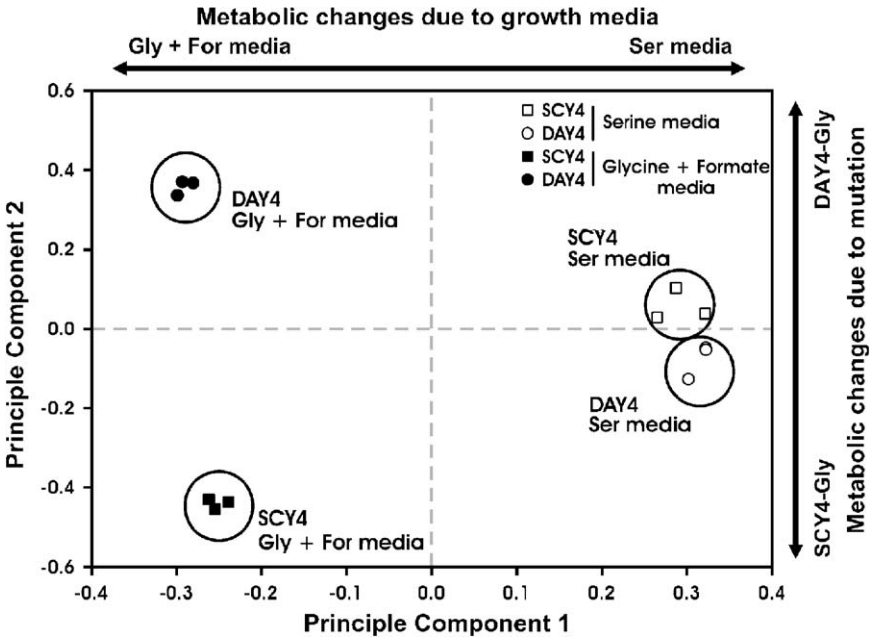

Fig. 9. "Basins of stability" in the yeast metabolome, as revealed by principle component analysis (PCA) of DAY4 and SCY4 metabolic profiles in different nutritional states. DAY4 and SCY4 metabolic states resemble each other in Ser media, but differ dramatically when shifted to Gly + For media. The relationships among the experiments are revealed by projecting the metabolic profiles of the 12 experimental samples onto the first two principle components. There are four clear groupings, with each biological triplicate clustering strongly, suggesting these states correspond to reproducibly accessible minima in the energetic landscape sampled by the metabolome. Principle component 1 corresponds largely to metabolic changes due to cell nutritional status, while principle component 2 corresponds largely to the genotype-dependent differences in the metabolome. These discrete metabolic states presumably correspond to "basins of stability" in the landscape of possible metabolite concentrations, representing preferred states of metabolism under these environmental and genotypic conditions.

The PCA analysis portrays a portion of the space of allowable metabolic states and can be interpreted as a metabolome phase diagram showing multiple dynamic steady states and the transitions between them. A change in the metabolic network, even one as subtle as the change of a single feedback loop, can produce large changes in the metabolome. Energetically, the effects of elevating levels of AdoMet propagate through the network, with successive metabolic reactions adjusting their flux in order to accommodate the perturbation. The perturbation is local, but serves to change the global balance of metabolites, driving the cell to a distinct metabolic state. Transitions between these distinct states are reproducible across biological replicates, and although some minor variations in state are observed, equivalent perturbations reproducibly drive the system to reproducible dynamic steady states. Thus, these states are stable solutions to the set of metabolic reactions, and the energetic landscape is such that accessible paths connect these states.

We observe variation in one of the metabolic states that is worth noting: the subtle metabolome variation between biological replicates of the SCY4-Gly + For cells. In particular, as shown in Fig. 4, the AdoMet level is higher in the first two samples than in the third sample, while glutathione (GSH) shows the inverse pattern. We believe this trend may reflect the regulation of homocysteine synthesis by cysteine. As shown in Fig. 5, homocysteine sits at a branch point: it can either be re-methylated with CH_3-THF to generate methionine and AdoMet, or condense with serine in the transsulfuration pathway to synthesize cysteine and GSH (Finkelstein and Martin, 1984; Ono et al., 1988). We cannot detect cysteine in our samples, but if we assume GSH and cysteine are in equilibrium, then cysteine is also higher in the third triplicate of SCY4 grown in glycine + formate medium. It has previously been shown that adenylylsulfate kinase (encoded by *MET14*) and *O*-acetylhomoserine (thiol)-lyase (encoded by *MET17*) are both negatively affected by cysteine (Hansen and Johannesen, 2000). These reactions are part of the sulfur assimilation pathway that produces homocysteine. Therefore, cysteine may in turn limit the levels of homocysteine available to accept the methyl group from CH_3-THF and, thus, contribute to the control of AdoMet accumulation. Indeed, it has been observed that addition of GSH in culture media completely blocks AdoMet accumulation in SCY4 grown in glycine + formate medium (Chan and Appling, 2003).

It therefore appears that the three replicate SCY4-Gly + For samples show discrete substates with reversed AdoMet/GSH ratios, such as might be caused from independent resolutions of a meta-stable state created by competing feedback inhibition loops. Interestingly, meta-stable metabolic states were foreseen by Max Delbrück in 1948, who described theoretically expected properties of such "systems in dynamic equilibrium", including the notion that in a situation where sets of enzymatic reactions

interact, a metabolic system might adopt multiple different states under identical conditions, passing between the states in response to "transitory perturbations" (Delbrück, 1948). Although the AdoMet/GSH observation requires more complete validation and characterization, we suggest this might prove an interesting system for exploring such metastability.

Finally, the observation of reasonably well-defined metabolic steady states gives some encouragement to the notion that it may be theoretically possible to model the life of a cell as a series of such transitions between dynamic steady states, provided it is feasible to experimentally map out the most common states sampled by growing cells. The number of such states is theoretically quite large (all possible combinations of the concentrations of metabolites, RNAs and proteins). However, a compelling argument can be made that a cell may only sample a limited subset of such states. In particular, many systems in the cell are tightly coupled, limiting the number of states sampled by the coupled systems, and many systems in the cell are feedback-regulated and therefore seek basins of energetic stability. These suggest it may indeed be feasible to characterize a cell by precisely defining trajectories of states through the process of normal cell growth, leading to simplified models of cell growth.

Acknowledgments

We thank Vishy Iyer and members of the Iyer lab for constructing and contributing the yeast whole genome DNA microarrays, and John Prince for help with mass spectrometry. This work was supported by grants from the N.S.F. (IIS-0325116, EIA-0219061, 0241180), N.I.H. (GM06779-01), Welch (F1515, F1353), and a Packard Fellowship (E.M.M.).

Appendix A

Raw DNA microarray and mass spectrometry shotgun proteomics data have been deposited into the Longhorn Array Database (Killion et al., 2003) and the Open Proteomics Database (Prince et al., 2004), respectively.

Appendix B. Supplementary Materials

Supplementary data associated with this article can be found in the online version at doi:10.1016/j.ymben.2006.06.003.

References

Aebersold, R., Mann, M., 2003. Mass spectrometry-based proteomics. Nature 422, 198–207.

Arnold, W.N., Lacy, J.S., 1977. Permeability of the cell envelope and osmotic behavior in *Saccharomyces cerevisiae*. J. Bacteriol. 131, 564–571.

Balasundaram, D., Tabor, C.W., Tabor, H., 1991. Spermidine or spermine is essential for the aerobic growth of *Saccharomyces cerevisiae*. Proc. Natl. Acad. Sci. USA 88, 5872–5876.

Chan, K.L., New, D., Ghandhi, S., Wong, F., Lam, C.M., Wong, J.T., 2002. Transcript levels of the eukaryotic translation initiation factor 5A gene peak at early G(1) phase of the cell cycle in the dinoflagellate *Crypthecodinium cohnii*. Appl. Environ. Microbiol. 68, 2278–2284.

Chan, S.Y., Appling, D.R., 2003. Regulation of *S*-adenosylmethionine levels in *Saccharomyces cerevisiae*. J. Biol. Chem. 278, 43051–43059.

Delaglio, F., Grzesiek, S., Vuister, G.W., Zhu, G., Pfeifer, J., Bax, A., 1995. NMRPipe: a multidimensional spectral processing system based on UNIX pipes. J. Biomol. NMR 6, 277–293.

Delbecq, P., Werner, M., Feller, A., Filipkowski, R.K., Messenguy, F., Pierard, A., 1994. A segment of mRNA encoding the leader peptide of the CPA1 gene confers repression by arginine on a heterologous yeast gene transcript. Mol. Cell. Biol. 14, 2378–2390.

Delbrück, M., 1948. Discussion, Unités Biologiques Douées de Continuité Génétique. Éditions du Centre National de la Recherche Scientifique, 1949, Paris, June–July, pp. 33–35.

Duda, P.O., Hart, P.E., Stork, D.G., 2001. Pattern Classification.

Eisen, M.B., Spellman, P.T., Brown, P.O., Botstein, D., 1998. Cluster analysis and display of genome-wide expression patterns. Proc. Natl. Acad. Sci. USA 95, 14863–14868.

Eng, J.K., McCormack, A.L., Yates 3rd, J.R., 1994. An approach to correlate tandem mass spectral data of peptides with amino acid sequences in a protein database. J. Am. Soc. Mass. Spectrom. 5, 976–989.

Fell, D., 1996. Understanding the Control of Metabolism. Ashgate Publishing.

Fiehn, O., Kopka, J., Dormann, P., Altmann, T., Trethewey, R.N., Willmitzer, L., 2000. Metabolite profiling for plant functional genomics. Nat. Biotechnol. 18, 1157–1161.

Finkelstein, J.D., Martin, J.J., 1984. Methionine metabolism in mammals. Distribution of homocysteine between competing pathways. Biol. Chem. 259, 9508–9513.

Fontecave, M., Atta, M., Mulliez, E., 2004. *S*-adenosylmethionine: nothing goes to waste. Trends Biochem. Sci. 29, 243–249.

Forster, J., Famili, I., Fu, P., Palsson, B.O., Nielsen, J., 2003. Genome-scale reconstruction of the *Saccharomyces cerevisiae* metabolic network. Genome Res. 13, 244–253.

Griffin, T.J., Gygi, S.P., Ideker, T., Rist, B., Eng, J., Hood, L., Aebersold, R., 2002. Complementary profiling of gene expression at the transcriptome and proteome levels in *Saccharomyces cerevisiae*. Mol. Cell. Proteomics 1, 323–333.

Hahn, J.S., Hu, Z., Thiele, D.J., Iyer, V.R., 2004. Genome-wide analysis of the biology of stress responses through heat shock transcription factor. Mol. Cell. Biol. 24, 5249–5256.

Hansen, J., Johannesen, P.F., 2000. Cysteine is essential for transcriptional regulation of the sulfur assimilation genes in *Saccharomyces cerevisiae*. Mol. Gen. Genet. 263, 535–542.

Ideker, T., Thorsson, V., Ranish, J.A., Christmas, R., Buhler, J., Eng, J.K., Bumgarner, R., Goodlett, D.R., Aebersold, R., Hood, L., 2001. Integrated genomic and proteomic analyses of a systematically perturbed metabolic network. Science 292, 929–934.

Ishihama, Y., Oda, Y., Tabata, T., Sato, T., Nagasu, T., Rappsilber, J., Mann, M., 2005. Exponentially Modified Protein Abundance Index (emPAI) for estimation of absolute protein amount in proteomics by the number of sequenced peptides per protein. Mol. Cell. Proteomics 4, 1265–1272.

Iyer, V.R., 2003. Isolation and amplification of array material from yeast. In: Bowtell, D., Sambrook, J. (Eds.), DNA Microarrays: A Molecular Cloning Manual. Cold Spring Harbor Press, Cold Spring Harbor, NY, pp. 30–34.

Kay, D.G., Singer, R.A., Johnston, G.C., 1980. Ornithine decarboxylase activity and cell cycle regulation in *Saccharomyces cerevisiae*. J. Bacteriol. 141, 1041–1046.

Keller, A., Nesvizhskii, A.I., Kolker, E., Aebersold, R., 2002. Empirical statistical model to estimate the accuracy of peptide identifications made by MS/MS and database search. Anal. Chem. 74, 5383–5392.

Killion, P.J., Sherlock, G., Iyer, V.R., 2003. The Longhorn Array Database (LAD): an open-source, MIAME compliant implementation of the Stanford Microarray Database (SMD). BMC Bioinform. 4, 32.

Kim, J., Iyer, V.R., 2004. Global role of TATA box-binding protein recruitment to promoters in mediating gene expression profiles. Mol. Cell. Biol. 24, 8104–8112.

Lindon, J.C., Holmes, E., Nicholson, J.K., 2003. So what's the deal with metabonomics? Anal. Chem. 75, 384A–391A.

Link, A.J., Eng, J., Schieltz, D.M., Carmack, E., Mize, G.J., Morris, D.R., Garvik, B.M., Yates III, J.R., 1999. Direct analysis of protein complexes using mass spectrometry. Nat. Biotechnol. 17, 676–682.

Liu, H., Sadygov, R.G., Yates III, J.R., 2004. A model for random sampling and estimation of relative protein abundance in shotgun proteomics. Anal. Chem. 76, 4193–4201.

Lockhart, D.J., Winzeler, E.A., 2000. Genomics, gene expression and DNA arrays. Nature 405, 827–836.

Lu, P., Nakorchevskiy, A., Marcotte, E.M., 2003. Expression deconvolution: a reinterpretation of DNA microarray data reveals dynamic changes in cell populations. Proc. Natl. Acad. Sci. USA 100, 10370–10375.

McNeil, J.B., McIntosh, E.M., Taylor, B.V., Zhang, F.R., Tang, S., Bognar, A.L., 1994. Cloning and molecular characterization of three genes, including two genes encoding serine hydroxymethyltransferases, whose inactivation is required to render yeast auxotrophic for glycine. J. Biol. Chem. 269, 9155–9165.

Messenguy, F., Feller, A., Crabeel, M., Pierard, A., 1983. Control-mechanisms acting at the transcriptional and post-transcriptional levels are involved in the synthesis of the arginine pathway carbamoylphosphate synthase of yeast. Embo J. 2, 1249–1254.

Mizunuma, M., Miyamura, K., Hirata, D., Yokoyama, H., Miyakawa, T., 2004. Involvement of S-adenosylmethionine in G1 cell-cycle regulation in *Saccharomyces cerevisiae*. Proc. Natl. Acad. Sci. USA 101, 6086–6091.

Nesvizhskii, A.I., Keller, A., Kolker, E., Aebersold, R., 2003. A statistical model for identifying proteins by tandem mass spectrometry. Anal. Chem. 75, 4646–4658.

Ono, B., Shirahige, Y., Nanjoh, A., Andou, N., Ohue, H., Ishino-Arao, Y., 1988. Cysteine biosynthesis in *Saccharomyces cerevisiae*: mutation that confers cystathionine beta-synthase deficiency. J. Bacteriol. 170, 5883–5889.

Parekh, R.B., Rohlff, C., 1997. Post-translational modification of proteins and the discovery of new medicine. Curr. Opin. Biotechnol. 8, 718–723.

Prince, J.T., Carlson, M.W., Wang, R., Lu, P., Marcotte, E.M., 2004. The need for a public proteomics repository. Nat. Biotechnol. 22, 471–472.

Raamsdonk, L.M., Teusink, B., Broadhurst, D., Zhang, N., Hayes, A., Walsh, M.C., Berden, J.A., Brindle, K.M., Kell, D.B., Rowland, J.J., Westerhoff, H.V., van Dam, K., Oliver, S.G., 2001. A functional genomics strategy that uses metabolome data to reveal the phenotype of silent mutations. Nat. Biotechnol. 19, 45–50.

Robinson, M.D., Grigull, J., Mohammad, N., Hughes, T.R., 2002. FunSpec: a web-based cluster interpreter for yeast. BMC Bioinform. 3, 35.

Roje, S., Chan, S.Y., Kaplan, F., Raymond, R.K., Horne, D.W., Appling, D.R., Hanson, A.D., 2002. Metabolic engineering in yeast demonstrates that *S*-adenosylmethionine controls flux through the methylenetetrahydrofolate reductase reaction in vivo. J. Biol. Chem. 277, 4056–4061.

Schwartz, B., Hittelman, A., Daneshvar, L., Basu, H.S., Marton, L.J., Feuerstein, B.G., 1995. A new model for disruption of the ornithine decarboxylase gene, SPE1, in *Saccharomyces cerevisiae* exhibits growth arrest and genetic instability at the MAT locus. Biochem. J. 312 (Pt 1), 83–90.

Shryock, J.C., Rubio, R., Berne, R.M., 1986. Extraction of adenine nucleotides from cultured endothelial cells. Anal. Biochem. 159, 73–81.

Spellman, P.T., Sherlock, G., Zhang, M.Q., Iyer, V.R., Anders, K., Eisen, M.B., Brown, P.O., Botstein, D., Futcher, B., 1998. Comprehensive identification of cell cycle-regulated genes of the yeast *Saccharomyces cerevisiae* by microarray hybridization. Mol. Biol. Cell 9, 3273–3297.

Strathern, J.N., Jones, E.W., Broach, J., 1982. The molecular biology of the yeast *Saccharomyces*: metabolism and gene expression. Cold Spring Harbor Laboratory Press, Cold Spring Harbor, NY.

Szyperski, T., Glaser, R.W., Hochuli, M., Fiaux, J., Sauer, U., Bailey, J.E., Wuthrich, K., 1999. Bioreaction network topology and metabolic flux ratio analysis by biosynthetic fractional ^{13}C labeling and two-dimensional NMR spectroscopy. Metab. Eng. 1, 189–197.

Tomitori, H., Kashiwagi, K., Asakawa, T., Kakinuma, Y., Michael, A.J., Igarashi, K., 2001. Multiple polyamine transport systems on the vacuolar membrane in yeast. Biochem. J. 353, 681–688.

Vanaerts, L.A., Blom, H.J., Deabreu, R.A., Trijbels, F.J., Eskes, T.K., Copius Peereboom-Stegeman, J.H., Noordhoek, J., 1994. Prevention of neural tube defects by and toxicity of L-homocysteine in cultured postimplantation rat embryos. Teratology 50, 348–360.

Viant, M.R., 2003. Improved methods for the acquisition and interpretation of NMR metabolomic data. Biochem. Biophys. Res. Commun. 310, 943–948.

Viant, M.R., Rosenblum, E.S., Tieerdema, R.S., 2003. NMR-based metabolomics: a powerful approach for characterizing the effects of environmental stressors on organism health. Environ. Sci. Technol. 37, 4982–4989.

Wang, R., Prince, J.T., Marcotte, E.M., 2005. Mass spectrometry of the M. smegmatis proteome: protein expression levels correlate with function, operons, and codon bias. Genome Res. 15, 1118–1126.

Washburn, M.P., Wolters, D., Yates III, J.R., 2001. Large-scale analysis of the yeast proteome by multidimensional protein identification technology. Nat. Biotechnol. 19, 242–247.

Werner, M., Feller, A., Messenguy, F., Pierard, A., 1987. The leader peptide of yeast gene CPA1 is essential for the translational repression of its expression. Cell 49, 805–813.

Woldman, Y., Appling, D.R., 2002. A general method for determining the contribution of split pathways in metabolite production in the yeast *Saccharomyces cerevisiae*. Metab. Eng. 4, 170–181.

Xue, Y., Bai, X., Lee, I., Kallstrom, G., Ho, J., Brown, J., Stevens, A., Johnson, A.W., 2000. *Saccharomyces cerevisiae* RAI1 (YGL246c) is homologous to human DOM3Z and encodes a protein that binds the nuclear exoribonuclease Rat1p. Mol. Cell. Biol. 20, 4006–4015.

Yi, E.C., Marelli, M., Lee, H., Purvine, S.O., Aebersold, R., Aitchison, J.D., Goodlett, D.R., 2002. Approaching complete peroxisome characterization by gas-phase fractionation. Electrophoresis 23, 3205–3216.